Gastric Cancer (2023) 26:169–186
https://doi.org/10.1007/s10120-022-01348-z

ORIGINAL ARTICLE

LOC101929709 promotes gastric cancer progression by aiding LIN28B to stabilize c-MYC mRNA

Tong-peng Xu[1] · Tao Yu[1] · Meng-yan Xie[1] · Yuan Fang[1] · Ting-ting Xu[1] · Yu-tian Pan[1] · Pei Ma[1] · Yong-qian Shu[1]

Received: 18 July 2022 / Accepted: 15 October 2022 / Published online: 25 October 2022

Abstract

Background LIN28B plays a critical role in the Warburg effect. However, its underlying mechanism remains elusive. Recently, it has been reported that LIN28B could collaborate with IGF2BP3, which can bind to m6A-modified c-MYC transcripts. Therefore, this study investigated if LIN28B recognises methylated c-MYC mRNA to promote the Warburg effect in gastric cancer.

Methods Effects of LIN28B on gastric cancer were confirmed in vitro and in vivo. On the basis of bioinformatics analysis, the association between LIN28B and c-MYC mRNA was shown using RNA immunoprecipitation (RIP) and luciferase reporter assays. The role of m6A was identified by RNA pull-down assays. We further performed RIP-seq to search for long non-coding RNAs (lncRNAs) participating in the LIN28B binding process. Chromatin immunoprecipitation was used to show the impact of c-MYC on transcription of LIN28B and lncRNAs.

Results LIN28B was identified to stabilize c-MYC mRNA by recognizing m6A. Furthermore, the interaction between c-MYC mRNA and LIN28B is speculated to be supported by LOC101929709, which binds to both LIN28B and IGF2BP3. Functional experiments revealed that LOC101929709 promotes the proliferation, migration and glycolysis of gastric cancer. Mechanistically, LOC101929709 enriched in the cytoplasm helps LIN28B stabilize c-MYC mRNA. Moreover, c-MYC promoted the transcription of both LOC101929709 and LIN28B. Additionally, LOC101929709 also activated the PI3K/AKT pathway.

Conclusions The c-MYC/LOC101929709/LIN28B axis promotes aerobic glycolysis and tumour progression. Thus, LOC101929709 can be a novel potential target for gastric cancer treatment.

Keywords LIN28B · LOC101929709 · c-MYC · Gastric cancer · The Warburg effect

Abbreviations

ANOVA	One-way analysis of variance
CDK2	Cyclin-dependent kinase 2
cDNAs	Complementary DNAs
CDS	Coding sequence
ChIP	Chromatin immunoprecipitation
Co-IP	Co-immunoprecipitation
CRD	Coding region determinant
CST	Cell signaling technology
ECAR	Extracellular acidification rate
FBS	Fetal bovine serum
FISH	Fluorescent in situ hybridization
GO	Gene ontology
HK2	Hexokinase 2
H3K4	Histone H3 lysines 4
IF	Immunofluorescence
IGF	Insulin-like growth factor
IGF2BP3	IGF2 mRNA binding protein 3
IHC	Immunohistochemical
KEGG	Kyoto Encyclopedia of Genes and Genomes
LncRNAs	Long non-coding RNAs
m6A	N6-methyladenosine
MAZ	MYC associated zinc finger protein
MERIP	Methylated RNA immunoprecipitation
miRNA	MicroRNA
NC	Negative control
MT	Mutant type
OCR	Oxygen consumption rate
OS	Overall survival
PDK1	Pyruvate dehydrogenase kinase

Tong-peng Xu, Tao Yu, Meng-yan Xie have contributed equally.

✉ Yong-qian Shu
yongqian_shu@163.com; shuyongqian@csco.org.cn

[1] Department of Oncology, the First Affiliated Hospital of Nanjing Medical University, No. 300 Guangzhou Road, Nanjing 210029, Jiangsu, People's Republic of China

RBP	RNA binding protein
RLU	Relative luciferase unit
RLUC	Renilla luciferase
RNP	Ribonucleoprotein
RIP	RNA immunoprecipitation
SDS-PAGE	SDS-polyacrylamide gel electrophoresis
WT	Wild type

Introduction

Gastric cancer is one of the most prevalent types of cancer, ranking second in cancer-related mortality worldwide [1]. Chemotherapy is the first-line treatment for progressive gastric cancer; however, drug resistance represses its efficacy. It has been reported that glycolysis is excessively activated in gastric cancer, even under normoxic conditions [2], and is known as the 'Warburg effect'. The Warburg effect not only supplies the necessary energy required for cancer progression but also reduces oxidative stress damage. Moreover, excessive lactate production can acidize the extracellular matrix and help tumour cells escape immune surveillance [3]. A series of enzymes, transcription factors (TFs) and signaling pathways collaborate to regulate the Warburg effect. For example, c-MYC, HIF-1α and p53 are three key TFs in glycolysis. They work with the PI3K/AKT pathway in regulating the expression of glycolytic enzymes [4]. Repressing the Warburg effect is expected to elicit a positive tumour inhibitory response with few adverse effects [2]. Inhibitors like 2-deoxy-D-glucose or 3-Bromopyruvate repress hexokinase 2 (HK2), showing promising therapeutic potential [5]. Hence, mutant metabolism is an ideal target for clinical intervention.

It is well-known that LIN28B participates in abnormal glucose metabolism [6]. LIN28B, an RNA binding protein (RBP), is highly expressed in human cancers and associated with poor prognosis [7, 8]. Its inhibition represses cancer proliferation and migration and induces apoptosis [9]. Tumour suppressor microRNA (miRNA) let-7 is a classic downstream target of LIN28B [10], which inhibits pyruvate dehydrogenase kinase (PDK1) and the PI3K/AKT pathway to attenuate aerobic glycolysis [11]. Conversely, LIN28B promotes glycolysis by inhibiting pri-let-7 and pre-let-7 maturation and activating HK1 and insulin-like growth factor (IGF). Moreover, LIN28B cooperates with c-MYC and contributes to tumour progression [12]. c-MYC reprograms metabolism by promoting the transcription of multiple glycolytic enzymes, including GLUT1, HK2, PDK1 and LDHA [13]. c-MYC also promotes LIN28B transcription [14]. Furthermore, a recent study reported that LIN28B accompanied by IGF2 mRNA binding protein 3 (IGF2BP3) directly binds to c-MYC mRNA [15]. The IGF2BP family can recognise RNA N6-methyladenosine (m6A) and subsequently stabilize c-MYC transcription [16]. In view of this mechanism, this study hypothesised that LIN28B is a potential candidate for the post-transcriptional modification of c-MYC via m6A recognition.

Long non-coding RNAs (lncRNAs) are pivotal regulators of biological processes [17]. An important function is guiding regulatory components to the target loci [18]. For example, lncRNA ROR guides hnRNP I and AUF1 together for c-MYC mRNA stabilization in breast cancer [19]. LncRNA TINCR binds to STAU1 and regulates KLF2 at the post-transcription level in gastric cancer [20]. Therefore, lncRNAs bound to both LIN28B and IGF2BP3 in gastric cancer cell lines were screened using RIP-seq and identifying their common peaks. LOC101929709 in chromosome 8q23.1 having a 1601 bp transcript was selected as the research object. These results revealed that LOC101929709 upregulated the expression of c-MYC, promoted tumour proliferation and migration and facilitated the Warburg effect. Thus, LOC101929709 could work in concert with LIN28B and c-MYC to form the c-MYC/LOC101929709/LIN28B axis, which can regulate the PI3K/AKT pathway and is beneficial for gastric cancer development.

Results

LIN28B promotes gastric cancer progression

Based on TCGA data, LIN28B was highly expressed in gastric cancer tissues compared with normal tissues. Prognoses of patients with gastric cancer having more LIN28B were worse than those with less LIN28B (Supplementary Fig. S1a, b). Furthermore, LIN28B was verified to be higher in gastric cancer cell lines (AGS, MKN1, SGC-7901, BGC-823 and MGC-803) than in the normal gastric cell line GES-1 using qRT-PCR and Western blot (Fig. 1A). Expression of LIN28B in cell lines was regulated by transfecting siRNAs or overexpression plasmids (Supplementary Fig. S1c, d). CCK-8 assays, colony formation assays and EdU staining revealed that LIN28B knockdown decreased tumour cell proliferation (Fig. 1B, C, Supplementary Fig. S3a). Additionally, wound healing and transwell assays showed that LIN28B knockdown reduced tumour cell migration rates (Fig. 1D, E). Thus, the expression and effect of LIN28B are conducive to tumour promotion.

LIN28B binds to c-MYC mRNA partially by recognising m6A

c-MYC/LIN28B axis is reported to be an important factor in tumour progression [12]. This study confirmed that c-MYC expression changed on LIN28B overexpression or knockdown (Fig. 2A). To explore the mechanism of LIN28B

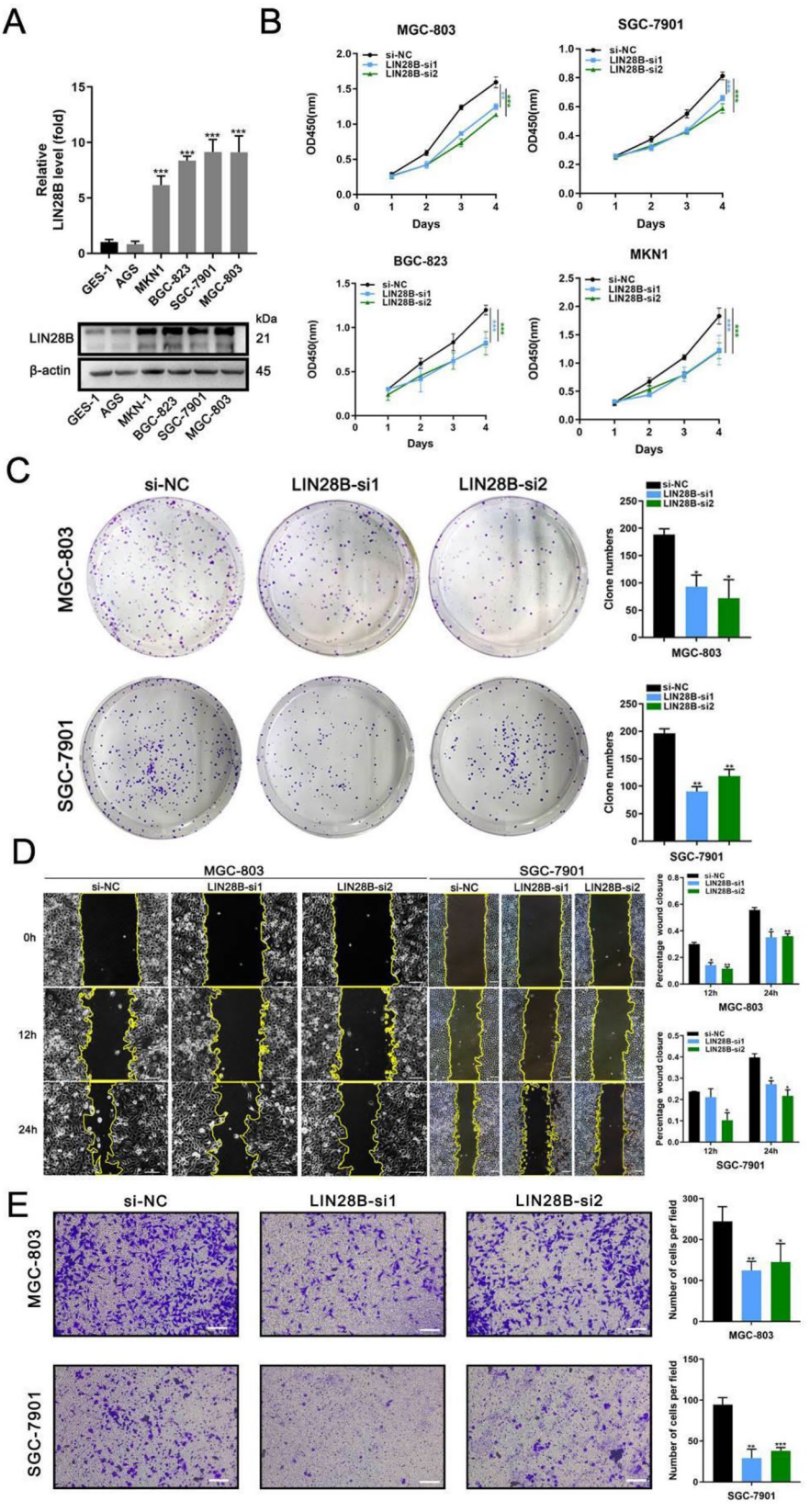

Fig. 1 LIN28B promotes gastric cancer progression. **A** LIN28B levels in GES-1, AGS, MKN1, SGC-7901, BGC-823 and MGC-803 are shown using real-time quantitative reverse transcription-polymerase chain reaction (qRT-PCR) and Western blot. **B**, **C** Growth curves from day 1 to 4 and colony formation assays show the proliferation of MGC-803, SGC-7901, BGC-823, and MKN1 transfected with si-NC or LIN28B-si1/2. Representative images of the crystal violet staining of cells in a 6-well plate. **D** Wound healing assays show scratches detected at 12 h and 24 h (10× magnification) to determine the migration of LIN28B knockdown in MGC-803/SGC-7901 cells. **E** Transwell assays show cells crossing the membrane dyed with crystal violet (10× magnification) to determine the migration of LIN28B knockdown in MGC-803/SGC-7901 cells. The data are presented as the mean of three independent experiments. Scale bars = 100 μm. $*p < 0.05$; $**p < 0.01$; $***p < 0.001$. Variables are presented as mean ± standard deviation (SD)

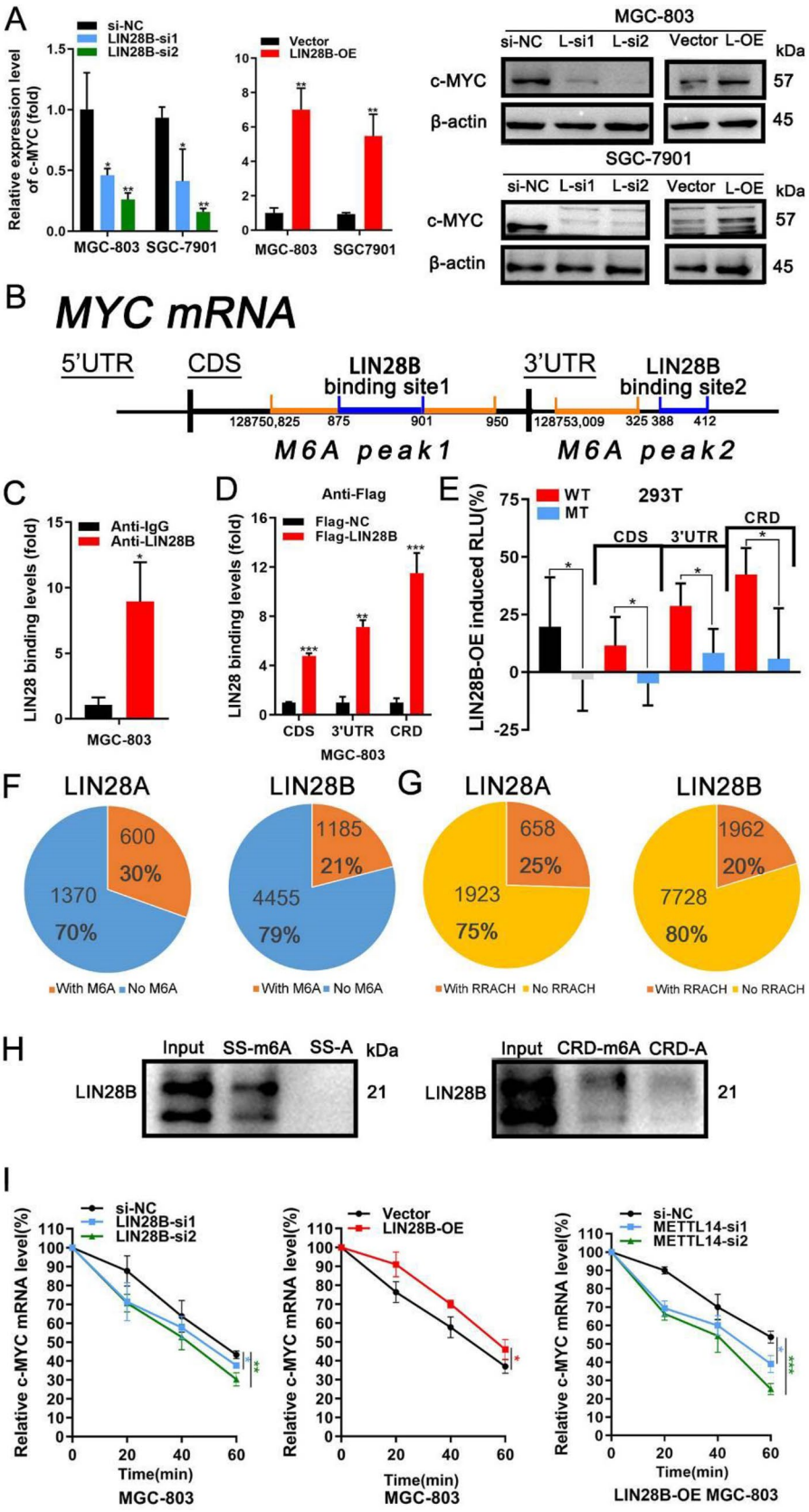
A
si-NC
LIN28B-si1
LIN28B-si2
Relative expression level of c-MYC (fold)
MGC-803 SGC-7901
Vector
LIN28B-OE
MGC-803 SGC7901
MGC-803
si-NC L-si1 L-si2 Vector L-OE kDa
c-MYC 57
β-actin 45
SGC-7901
si-NC L-si1 L-si2 Vector L-OE kDa
c-MYC 57
β-actin 45
B
MYC mRNA
5'UTR CDS LIN28B binding site1 3'UTR LIN28B binding site2
128750,825 875 901 950 128753,009 325 388 412
M6A peak1 M6A peak2
C
Anti-IgG
Anti-LIN28B
LIN28 binding levels (fold)
MGC-803
D
Anti-Flag
Flag-NC
Flag-LIN28B
LIN28 binding levels (fold)
CDS 3'UTR CRD
MGC-803
E
WT
MT
293T
CDS 3'UTR CRD
LIN28B-OE induced RLU(%)
F
LIN28A
600 30%
1370 70%
With M6A No M6A
LIN28B
1185 21%
4455 79%
With M6A No M6A
G
LIN28A
658 25%
1923 75%
With RRACH No RRACH
LIN28B
1962 20%
7728 80%
With RRACH No RRACH
H
Input SS-m6A SS-A kDa
LIN28B 21
Input CRD-m6A CRD-A
LIN28B 21
I
si-NC
LIN28B-si1
LIN28B-si2
Relative c-MYC mRNA level(%)
Time(min)
MGC-803
Vector
LIN28B-OE
Relative c-MYC mRNA level(%)
Time(min)
MGC-803
si-NC
METTL14-si1
METTL14-si2
Relative c-MYC mRNA level(%)
Time(min)
LIN28B-OE MGC-803

◂**Fig. 2** LIN28B binds to c-MYC mRNA partially by recognising m6A. **A** Expression of c-MYC in MGC-803/SGC-7901 transfected with si-NC, LIN28B-si1/2, vector or LIN28B-OE is shown using qRT-PCR (left) and Western blot (right). **B** Predicted LIN28B binding sites in c-MYC transcripts according to PAR-CLIP data are marked in blue. Sequences with potential m6A modification are marked in orange. **C** RIP assay using LIN28B antibody shows the association of c-MYC mRNA with LIN28B in MGC-803. **D** RIP assay using Flag antibody shows the binding between Flag-labelled LIN28B and different c-MYC mRNA parts (CDS, 3′UTR and CRD) in MGC-803. **E** Luciferase reporter assays show the association between LIN28B and different c-MYC mRNA (CRD, 3′UTR, and CRD) parts or their mutant types (MT) in 293 T viaRLU. The association of LIN28B with arid3A 3′UTR or its mutant type serves as a positive control (PC) or NC, respectively. **F** Pie charts show genes bound by LIN28A or LIN28B according to PAR-CLIP data. Orange parts comprise genes with m6A according to MERIP data (LIN28A: 600, 30%; LIN28B: 1185, 21%). Blue parts comprise genes without m6A (LIN28A: 1370, 70%; LIN28B: 4455, 79%). **G** Pie charts show sequences bound by LIN28A or LIN28B. Orange parts consist of sequences with the -RRACH- motif (LIN28A: 658, 25%; LIN28B: 1962, 20%). Yellow parts show sequences without -RRACH- (LIN28A: 1923, 75%; LIN28B: 7728, 80%). **H** Biotin-labelled RNA pull-down and western blot assays in MGC-803 show the binding between LIN28B and synthetic RNA fragments (single-stranded RNA bait SS-m6A/SS-A, or CRD-m6A/CRD). **I** After actinomycin D treatment, c-MYC mRNA is detected at indicated time points in MGC-803 transfected with si-NC/LIN28B-si1/2 (left), or with vector/LIN28B-OE (middle) or LIN28B-OE MGC-803 with si-NC or siRNA1/2 of the m6A writer METTL14 (right). The data are presented as the mean of three independent experiments. Scale bars = 100 μm. $*p < 0.05$; $**p < 0.01$; $***p < 0.001$. Variables are presented as mean ± SD

regulating c-MYC, published PAR-CLIP data of LIN28B was utilised [15, 21, 22]. Sequencing results showed LIN28B binding sites on the c-MYC coding sequence (CDS) and 3′ untranslated region (UTR) (Fig. 2B). RIP confirmed that LIN28B is bound to c-MYC mRNA (Fig. 2C). Moreover, flag-labelled exogenous LIN28B was shown to bind to CDS and 3′UTR (Fig. 2D). Furthermore, luciferase reporter assays showed that LIN28B only binds to the wild type (WT) of c-MYC mRNA instead of their mutant types (MT) (Fig. 2E). Thus, LIN28B is capable of binding to c-MYC mRNA.

Notably, m6A was found to be enriched in the binding sites of either LIN28A or LIN28B on comparing PAR-CLIP data with published methylated RNA immunoprecipitation (MERIP) sequencing results [23], suggesting that LIN28 proteins are potential m6A-binding proteins (Fig. 2F, G). Additionally, LIN28B RIP-seq revealed that part of LIN28B binding sites had the m6A consensus sequence, -RRACH- motif (R = G or A; H = A, C or U) [24], suggesting that LIN28B is a possible m6A reader (Supplementary Fig. S2a). Therefore, m6A was hypothesised to help LIN28B bind to mRNA. Subsequently, LIN28B was found to bind with a single-stranded RNA bait with m6A modification (ss-m6A) instead of unmethylated control RNA (ss-A) using RNA pull-down assays (Fig. 2H). Accordingly, the c-MYC coding region determinant (CRD), which possesses abundant m6A was found to be colocalized with LIN28B in MGC-803 shown using immunofluorescence (IF) (Supplementary Fig. S2c). Similarly, synthetic CRD RNA oligos with m6A (CRD-m6A) bind to more LIN28B than CRD without m6A (Fig. 2H). Moreover, IGF2BP3 could bind m6A-modified RNA (Supplementary Fig. S2e). Conversely, LIN28B could bind to CRD, and this binding was significantly inhibited upon the m6A writer (METTL3 or METTL14) knockdown (Supplementary Fig. S2d). Furthermore, LIN28B knockdown accelerated c-MYC mRNA degradation, suggesting that LIN28B regulated c-MYC at the post-transcription level (Fig. 2I). Additionally, METTL14 knockdown by siRNA modified c-MYC mRNA stability even in MGC-803 with ectopic LIN28B expression (Fig. 2I). In principle, m6A was speculated to play a crucial role in guiding RBPs, such as LIN28B and IGF2BP, to CRD to maintain c-MYC mRNA stability.

LIN28B regulates glycolysis partially through c-MYC

The relationship between c-MYC and LIN28B was further investigated using the c-MYC inhibitors (10,058-F4 and 10,074-G5, 15 μM) [25, 26]. LIN28B overexpression accelerated cell proliferation and migration (Supplementary Fig. S3c–e). c-MYC inhibition neutralized the tumour-promoting function of LIN28B upregulation, suggesting that LIN28B facilitated gastric cancer development, at least in part, via c-MYC (Fig. 3A–C, Supplementary Fig. S3b).

As c-MYC is a key regulator in the Warburg effect, its effect on LIN28B in glycolysis was investigated. LIN28B downregulation reduced glucose consumption and lactate acid production (Fig. 3D). Similarly, alterations of ECAR/OCR indicated that LIN28B knockdown impaired glycolytic reserves and promoted spare respiratory capacity (Fig. 3E). Conversely, LIN28B upregulation promoted the Warburg effect (Supplementary Fig. S3f), whereas c-MYC inhibition repressed glycolysis induced by LIN28B (Fig. 3F, G). Thus, it can be concluded from these results that the glycolysis-promoting effects of LIN28B partially originate from c-MYC.

LOC101929709 serves as a potential scaffold for LIN28B

lncRNAs are capable of reinforcing the interaction of proteins with transcripts [27]. To determine the elements involved in the LIN28B/c-MYC mRNA complex, RIP-seq using LIN28B and IGF2BP3 antibodies was conducted as they can form a ribonucleoprotein (RNP) complex to cooperatively stabilize mRNA [15, 16]. Additionally, the colocalization between LIN28B and IGF2BP3 in MGC-803 was observed (Supplementary Fig. S4a–c). LOC101929709 and

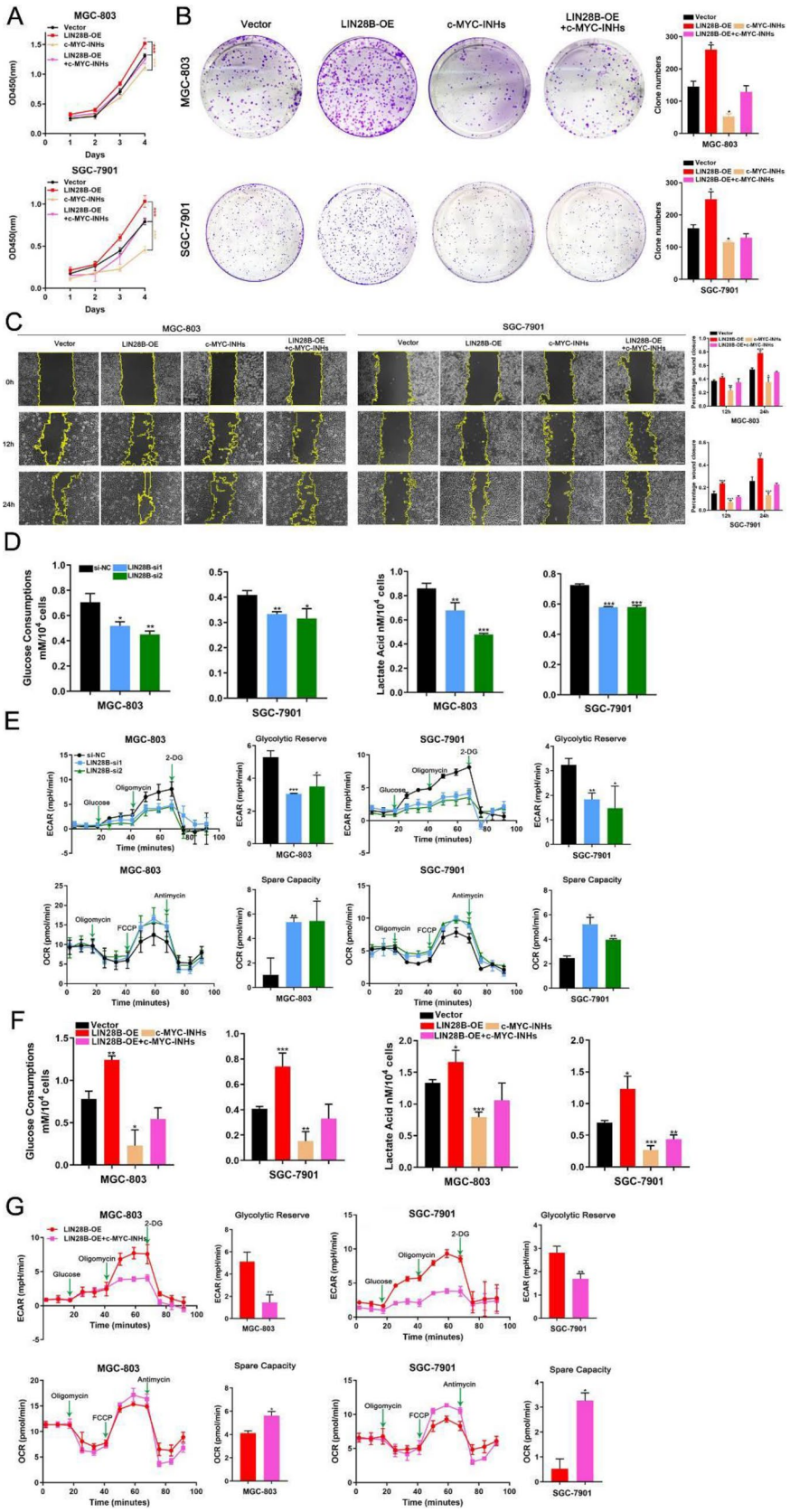

Fig. 3 LIN28B regulates glycolysis partially through c-MYC. **A**, **B** Growth curves from day 1 to 4 and colony formation assays show the proliferation of MGC-803/SGC-7901 with vector, LIN28B-OE, c-MYC-INHs and LIN28B-OE + c-MYC-INHs. 10,058-F4 and 10,074-G5 were used at 15 μM for in vitro experiments. **C** Wound healing assays show scratches detected at 12 h and 24 h to determine the migration of the above four groups. **D** The glucose uptake and lactic acid production of si-NC/LIN28B-si1/2 transfected MGC-803/SGC-7901 after 24 h. **E** Seahorse tracing curves and ECAR/OCR bars show the glycolytic reserve and spare respiratory capacity of si-NC/LIN28B-si1/2 transfected MGC-803/SGC-7901. **F** The glucose uptake and lactic acid production of MGC-803/SGC-7901 with vector, LIN28B-OE, c-MYC-INHs and LIN28B-OE + c-MYC-INHs after 24 h. **G** Seahorse tracing curves and ECAR/OCR bars show the glycolytic reserve and spare respiratory capacity of MGC-803/SGC-7901 with LIN28B-OE and LIN28B-OE + c-MYC-INHs. The data are presented as the mean of three independent experiments. Scale bars = 100 μm. $^{*}p < 0.05$; $^{**}p < 0.01$; $^{***}p < 0.001$. Variables are presented as mean ± SD

LINC01111 were also studied as they bind to both LIN28B and IGF2BP3 (Fig. 4A, Supplementary Table S2). Moreover, LOC101929709 was selected as the target owing to its high expression in gastric cancer cell lines and induction by c-MYC (Fig. 4B). Based on the GDC-TCGA database, LOC101929709 showed significantly higher expression in gastric cancer tissues than that in normal tissues (Supplementary Fig. S4e). Notably, the expression of LINC01111 in GES-1 or gastric cancer cell lines was similar (Supplementary Fig. S4d). RNA pull-down proved that LOC101929709 was capable of binding LIN28B and IGF2BP3 (Fig. 4C). Correspondingly, LIN28B and IGF2BP3 could bind to LOC101929709 in MGC-803, and the binding was enhanced on LOC101929709 overexpression (Fig. 4D, Supplementary Fig. S4f). The binding between LIN28B and LOC101929709 was also confirmed by RNA pull down and RIP assays in SGC-7901 and BGC-823 (Supplementary Fig. S4g). IF staining and nuclear/cytoplasmic separation experiments both verified the cytoplasmic distribution of LOC101929709 (Fig. 4E, F). Furthermore, IF showed that LOC101929709 was co-localized with LIN28B and IGF2BP3 (Fig. 4F). The expression of let-7c and let-7g, which are downstream effectors of LIN28B, was affected by the overexpression or knockdown of LOC101929709; however, luciferase reporter assays could not reveal that LOC101929709 directly binds to let-7 (Supplementary Fig. S4h–i). These results suggested that LOC101929709 participated in the binding between LIN28B and c-MYC mRNA in a let-7-independent manner.

LOC101929709 functions as an oncogenic lncRNA in vitro

LOC101929709 overexpression (L-OE) or knockdown cell lines were constructed, and their expression was verified (Supplementary Fig. S5a). Proliferation and migration abilities were decreased in LOC101929709 knockdown groups. (Fig. 5A–D, Supplementary Fig. S5b). Moreover, LOC101929709 knockdown caused G1 arrest, whereas LOC101929709-OE cells had a longer S phase (Fig. 5E). The expression of Cyclin-dependent kinase 2 (CDK2) and cyclin A, which are essential for S phase completion and DNA replication [28], was proportional to that of LOC101929709 (Fig. 5F). Hence LOC101929709 has the potential to accelerate the G1/S phase transition, thereby extending the S phase and promoting gastric cancer growth. Furthermore, LOC101929709 knockdown attenuated the glycolytic process, resulting in less glucose uptake, lactate acid production and glycolytic reserve (Fig. 5G, H). On the contrary, LOC101929709 overexpression promoted growth, migration, and glycolysis of AGS (Supplementary Fig. S5d–g). Therefore, it can be concluded from these results that LOC101929709 acts as an oncogenic lncRNA in gastric cancer.

LOC101929709 promotes tumour development via LIN28B

LOC101929709 might act as a scaffold to facilitate tumour development through LIN28B. LOC101929709 overexpression was conducive to cell viability, migration and aerobic glycolysis in MGC-803, which was counteracted by LIN28B-si1/2 (Fig. 6A–D, Supplementary Fig. S5c). Based on the RIP-seq results, LIN28B acts in tandem with metabolic pathways, such as the PI3K/AKT pathway and mTOR signaling pathway (Supplementary Fig. S6a). It is well-known that LIN28B mediates the activation of the PI3K/AKT pathway to regulate the hallmarks of cancer [29]. Thus, the PI3K/AKT pathway could be a potential downstream effector of the LOC101929709/LIN28B axis. The PI3K/AKT pathway is also affected by c-MYC [30]. Therefore, inhibiting AKT or c-MYC could mutually downregulate their expression and suppress the Warburg effect (Supplementary Fig. S6c–d). Furthermore, the expression of PI3K, p-AKT, p-mTOR and c-MYC was found to be inhibited on LOC101929709 knockdown but increased on its overexpression (Fig. 6E–F). This suggested that LOC101929709 could indirectly regulate c-MYC and the PI3K/AKT pathway via LIN28B to enhance cancer progression.

c-MYC induces LIN28B transcription by binding to the first intron of LIN28B [14]. Thus, this mechanism was validated using ChIP (Supplementary Fig. S6e). Upon c-MYC stimulation, the mutant of LIN28B first intron (LIN28B-INT1-MT) exhibited a markedly lower relative luciferase unit (RLU) than the wild type (Supplementary Fig. S6f). c-MYC can bind over 10–15% of all promoters [31], thus, the upstream sequences of LOC101929709 were further analysed by 2000 bp, and a putative binding site of c-MYC was predicted [32] (Fig. 6G). ChIP analysis using c-MYC antibodies was also performed to confirm the binding of c-MYC and LOC101929709 promoter (Fig. 6H). Luciferase reporter assays showed the increased activity of LOC101929709 promoter that was induced by c-MYC and subsequently inhibited by c-MYC inhibitors (Fig. 6I). Furthermore, the mutant of LOC101929709 promoter significantly decreased its RLU even with c-MYC stimulation (Fig. 6J). These results suggested that c-MYC promoted LOC101929709 transcription.

LOC101929709 functions as a bridge between LIN28B and c-MYC mRNA. The co-localization of LOC101929709 and CRD-m6A was shown using IF in MGC-803 (Fig. 6K). In LOC101929709-OE cells, c-MYC mRNA was found to be highly enriched in LIN28B immunoprecipitates (Fig. 6L). Thus, upregulating LOC101929709 could further raise RLU generated by LIN28B and c-MYC mRNA binding (Fig. 6M). Furthermore, LOC101929709 overexpression increased the stability of c-MYC mRNA, which was inhibited on LIN28B knockdown (Fig. 6N). These results suggested

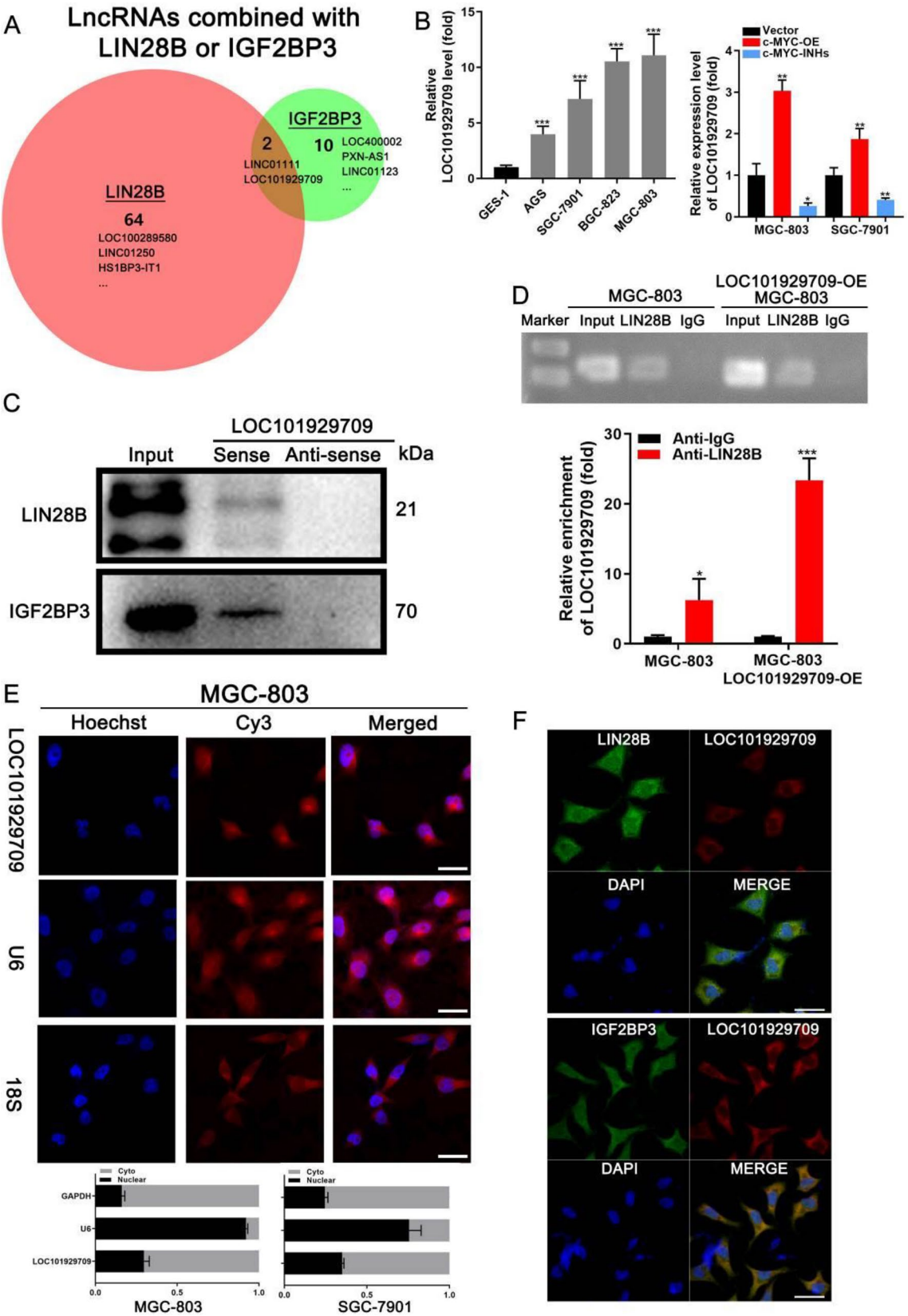
A
LncRNAs combined with LIN28B or IGF2BP3
LIN28B
64
LOC100289580
LINC01250
HS1BP3-IT1
...
IGF2BP3
2
LINC01111
LOC101929709
10
LOC400002
PXN-AS1
LINC01123
...
B
Relative LOC101929709 level (fold)
GES-1
AGS
SGC-7901
BGC-823
MGC-803
Vector
c-MYC-OE
c-MYC-INHs
Relative expression level of LOC101929709 (fold)
MGC-803
SGC-7901
C
LOC101929709
Input
Sense
Anti-sense
kDa
LIN28B
21
IGF2BP3
70
D
MGC-803
LOC101929709-OE MGC-803
Marker
Input LIN28B IgG
Input LIN28B IgG
Anti-IgG
Anti-LIN28B
Relative enrichment of LOC101929709 (fold)
MGC-803
MGC-803 LOC101929709-OE
E
MGC-803
Hoechst
Cy3
Merged
LOC101929709
U6
18S
Cyto
Nuclear
GAPDH
U6
LOC101929709
MGC-803
SGC-7901
F
LIN28B
LOC101929709
DAPI
MERGE
IGF2BP3
LOC101929709
DAPI
MERGE

◂**Fig. 4** LOC101929709 serves as a potential scaffold for LIN28B. **A** The Venn Diagram shows the potential lncRNAs bound to LIN28B ($n=64$) or IGF2BP3 ($n=10$), and their intersection (LINC01111 and LOC101929709) according to RIP-seq results in MGC-803. **B** The expression of LOC101929709 in GES-1, AGS, SGC-7901, BGC-823 and MGC-803 (left), and its expression upon c-MYC overexpression or inhibition (right) is shown using qRT-PCR. **C** RNA pull-down analysis followed by Western blot shows that the biotin-labelled sense strand of LOC101929709 binds to LIN28B and IGF2BP3 in MGC-803 but the anti-sense strand did not show any binding between them. **D** LOC101929709 was significantly enriched in LIN28B immunoprecipitates relative to the IgG in MGC-803 with or without LOC101929709 overexpression as shown using qRT-PCR. **E** Representative images of LOC101929709 localization in MGC-803 were detected using FISH (40×magnification). The left panel shows the nuclei stained with Hoechst. The middle shows LOC101929709, U6 or 18S stained with Cy3. The right panel shows the merged result (upper). The expression of LOC101929709 in the nucleus and cytoplasm is shown using qRT-PCR with GAPDH/U6 as the positive control (lower). **F** Distribution of LOC101929709 (red) and LIN28B or IGF2BP3 (green) and their co-localization in the cytoplasm of MGC-803 (40×magnification). The data are presented as the mean of three independent experiments. Scale bars = 100 μm. $^{*}p<0.05$; $^{**}p<0.01$; $^{***}p<0.001$. Variables are presented as mean ± SD

that LOC101929709 could aid LIN28B to stabilize c-MYC mRNA.

LOC101929709 promotes gastric cancer progression in vivo

Based on the TCGA stomach adenocarcinoma cohort, LOC101929709 was slightly positively associated with LIN28B ($n=371$, correlation coefficient = 0.09, $p=0.0574$). The association was also confirmed in two GEO cohorts consisting of advanced gastric cancer tissues ($n=172$, correlation coefficient = 0.14, $p=0.0624$; $n=322$, correlation coefficient = 0.11, $p=0.0520$) (Supplementary Fig. 7a). We conducted IHC and FISH analysis to determine the expression of LIN28B, IGF2BP3, and LOC101929709 in 25 pairs of gastric cancer tissues and matched adjacent normal tissues (Supplementary Table S3). LOC101929709 was upregulated in gastric cancer tissues compared with normal tissues (Fig. 7A). Its expression was positively associated with that of both LIN28B and IGF2BP3 ($n=25$, correlation coefficient = 0.30, $p=0.1519$; correlation coefficient = 0.14, $p=0.500$). Although the association was not significant due to the small sample size, results suggested that LOC101929709 might cooperate with LIN28B in gastric cancer.

An athymic (nu/nu) mouse model was constructed by injecting modified MGC-803 into the left flank or the tail vein of the mouse. Tumours grown from LOC101929709-OE cells were significantly heavier than those from the control group, which was consistent with the growth curve (Fig. 7B). Similarly, more pulmonary metastasis sites were detected in the LOC101929709-OE group (Fig. 7C). Western blot showed that the proteins involved in the PI3K/AKT pathway (p-mTOR, mTOR, PI3K, p-AKT and AKT), and c-MYC were found to be partly upregulated in the primary tumours of the LOC101929709-OE group (Fig. 7D). Tumours from the LOC101929709-OE group also exhibited a high c-MYC and Ki-67 index (Fig. 7E). On the other hand, the LOC101929709 knockdown models showed downregulated proliferation and metastasis abilities (Supplementary Fig. S7b, c). Correspondingly, oncogenic proteins (p-mTOR, PI3K, p-AKT, and c-MYC) were decreased in LOC101929709 knockdown subcutaneous tumours (Supplementary Fig. S7d). Reduction of c-MYC was also confirmed by IHC and qRT-PCR (Supplementary Fig. S7e). Additionally, the unprocessed gel blots are presented in Supplementary Figure S8. Finally, in vivo experiments showed that LOC101929709 promoted gastric cancer progression through the PI3K/AKT pathway and c-MYC.

Discussion

Reprogramming energy metabolism is an emerging hallmark of cancer [33]. The Warburg effect, which was identified by Otto Warburg in the 1920s, especially provides multiple benefits for solid tumours including gastric cancer [34]. Distinctive TFs and signaling pathways are involved in the Warburg effect [35]. In this study, the role of LIN28B in abnormal glucose metabolism was investigated. LIN28B, an oncogenic gene, was confirmed to promote the proliferation, migration and aerobic glycolysis of gastric cancer cells. Moreover, it participates in the regulation of various oncogenic factors. LIN28B represses let-7 to upregulate STAT3, HMGA2 and c-MYC [10, 36]. Moreover, LIN28B acts as an RBP and binds to the transcripts of MYC-associated zinc finger protein (MAZ) and IGF2BP, which affect c-MYC transcription [37]. Therefore, rescue experiments were designed, which identified that c-MYC is a key downstream effector of LIN28B.

Recent studies have reported that LIN28B along with IGF2BP3 could directly bind to c-MYC mRNA in mouse-derived hematopoietic cells [15, 38]. Therefore, LIN28B was speculated to be capable of post-transcriptionally regulating c-MYC. Results showed that LIN28B binds to the CDS and 3′UTR of c-MYC mRNA and increases its stability. Additionally, LIN28B was particularly enriched in the CRD region, which comprises the last 249 nucleotides of c-MYC CDS, with abundant m6A modification and was found to be responsible for recruiting endonucleases to degrade c-MYC transcriptions. Additionally, knocking down the m6A writer METTL3 or METTL14 inhibited the association between CRD and LIN28B, which was consistent with the finding that RBP-like IGF2BP connects with the CRD by recognising m6A to regulate c-MYC

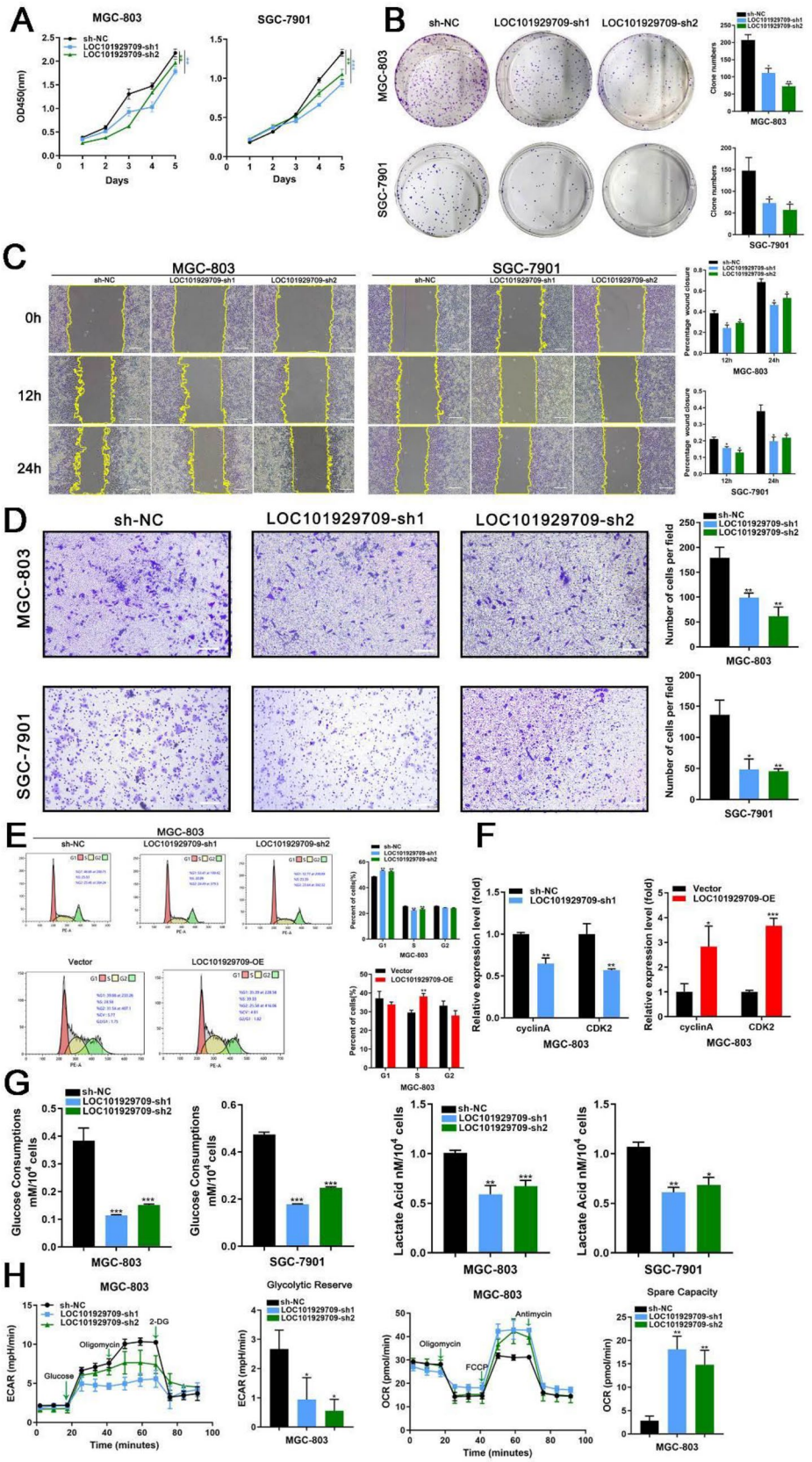

Fig. 5 LOC101929709 functions as an oncogenic lncRNA in vitro. **A**, **B** Growth curves from day 1 to 5 and colony formation assays show the proliferation of MGC-803/SGC-7901 with sh-NC or LOC101929709-sh1/2. **C** Wound healing assays show scratches detected at 12 h and 24 h to determine the migration of the above three groups. **D** Transwell assays show cells crossing the membrane dyed with crystal violet to determine the migration of LOC101929709 knockdown in MGC-803/SGC-7901 cells. **E** Proportions of the G1/S/G2 phase of the LOC101929709-OE/-sh1/2 groups are shown using FACS analysis. **F** Expression of cyclin A and CDK2 in MGC-803 with LOC101929709-OE/sh1 is shown using qRT-PCR. **G** The glucose uptake and lactic acid production of MGC-803/SGC-7901 with sh-NC or LOC101929709-sh1/2 after 24 h. **H** Seahorse tracing curves and ECAR/OCR bars of MGC-803 with sh-NC or LOC101929709-sh1/2. The data are presented as the mean of three independent experiments. Scale bars = 100 μm. $*p < 0.05$; $**p < 0.01$; $***p < 0.001$. Variables are presented as mean ± SD

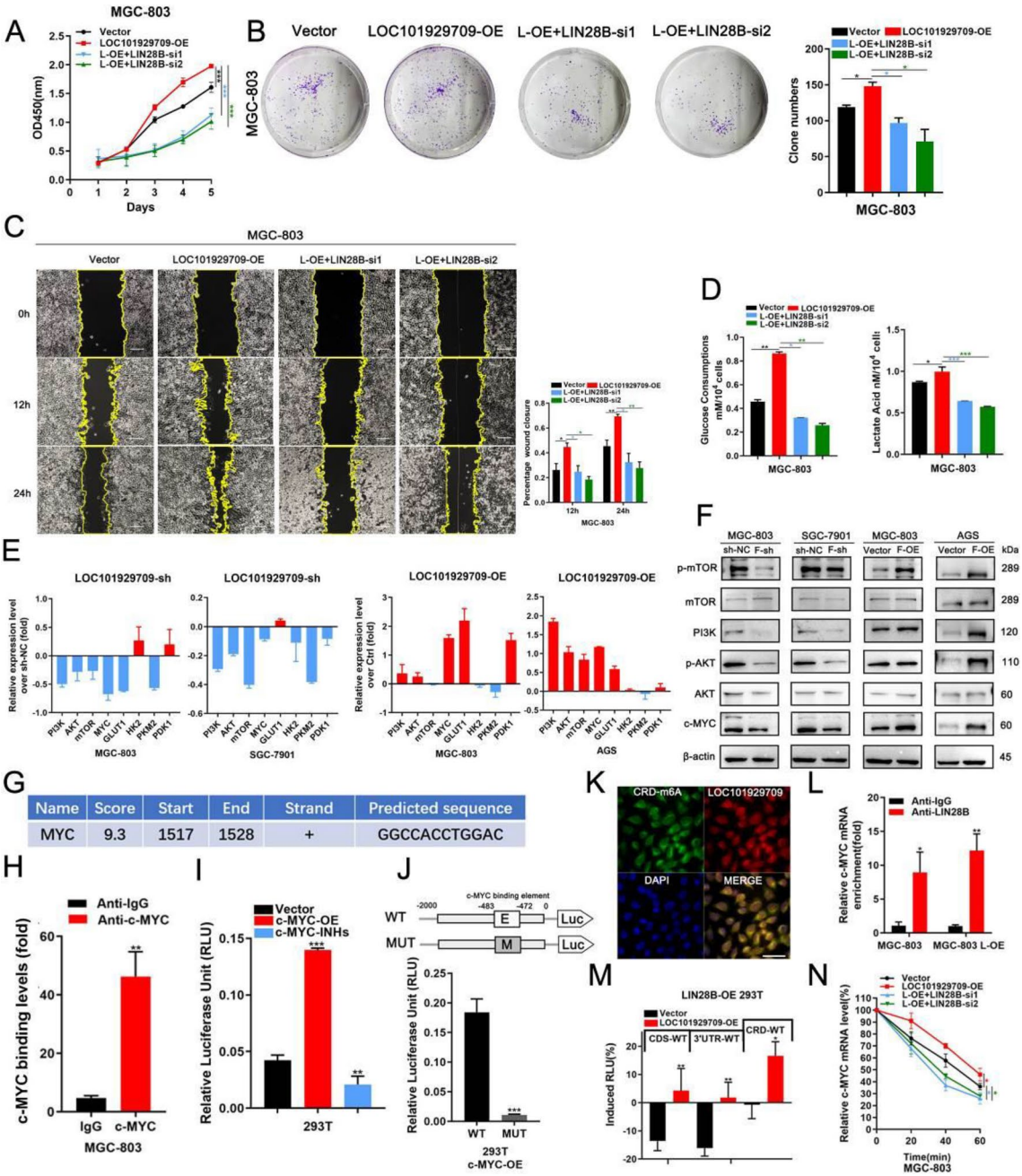

Fig. 6 LOC101929709 promotes tumour development via LIN28B. **A**, **B** Growth curves from day 1 to 5 and colony formation assays show the proliferation of LOC101929709-OE, LOC101929709-OE with LIN28B-si1/2 and NC groups. **C** Wound healing assays show scratches detected at 12 h and 24 h to determine the migration of the above four groups. **d** The glucose uptake and lactic acid production of the above four groups after 24 h. **E**, **F** Differently expressed mRNAs and proteins between the LOC101929709-sh/-OE and negative control (NC) groups in MGC-803, SGC-7901, and AGS are shown using qRT-PCR and Western blot. **G** The c-MYC binding sequence of the LOC101929709 promoter is predicted using JASPAR. **H** The promoter of LOC101929709 is immunoprecipitated using IgG or c-MYC antibody. **I** The binding between c-MYC and LOC101929709 promoter in the 293 T on c-MYC overexpression or inhibition is shown by RLU. **J** The association between c-MYC and the wild/mutant promoter of LOC101929709 (WT/MUT) is shown using RLU. **K** Distribution of LOC101929709 (red) and CRD-m6A (green) and their co-localization in the cytoplasm of MGC-803 (40×magnification). **L** c-MYC mRNA is significantly enriched in LIN28B immunoprecipitates compared to IgG in MGC-803 and LOC101929709-OE MGC-803 shown using RIP-PCR. **M** The association of LIN28B with CRD, 3′UTR and CRD of c-MYC in 293 T and LOC101929709-OE 293 T are shown via RLU. **N** After actinomycin D treatment, the expression of c-MYC mRNA is shown using qRT-PCR at indicated time points in MGC-803 transfected for 24 h with vector, LOC101929709-OE or LOC101929709-OE with LIN28B-si1/2. The data are presented as the mean of three independent experiments. Scale bars = 100 μm. $*p<0.05$; $**p<0.01$; $***p<0.001$. Variables are presented as mean ± SD

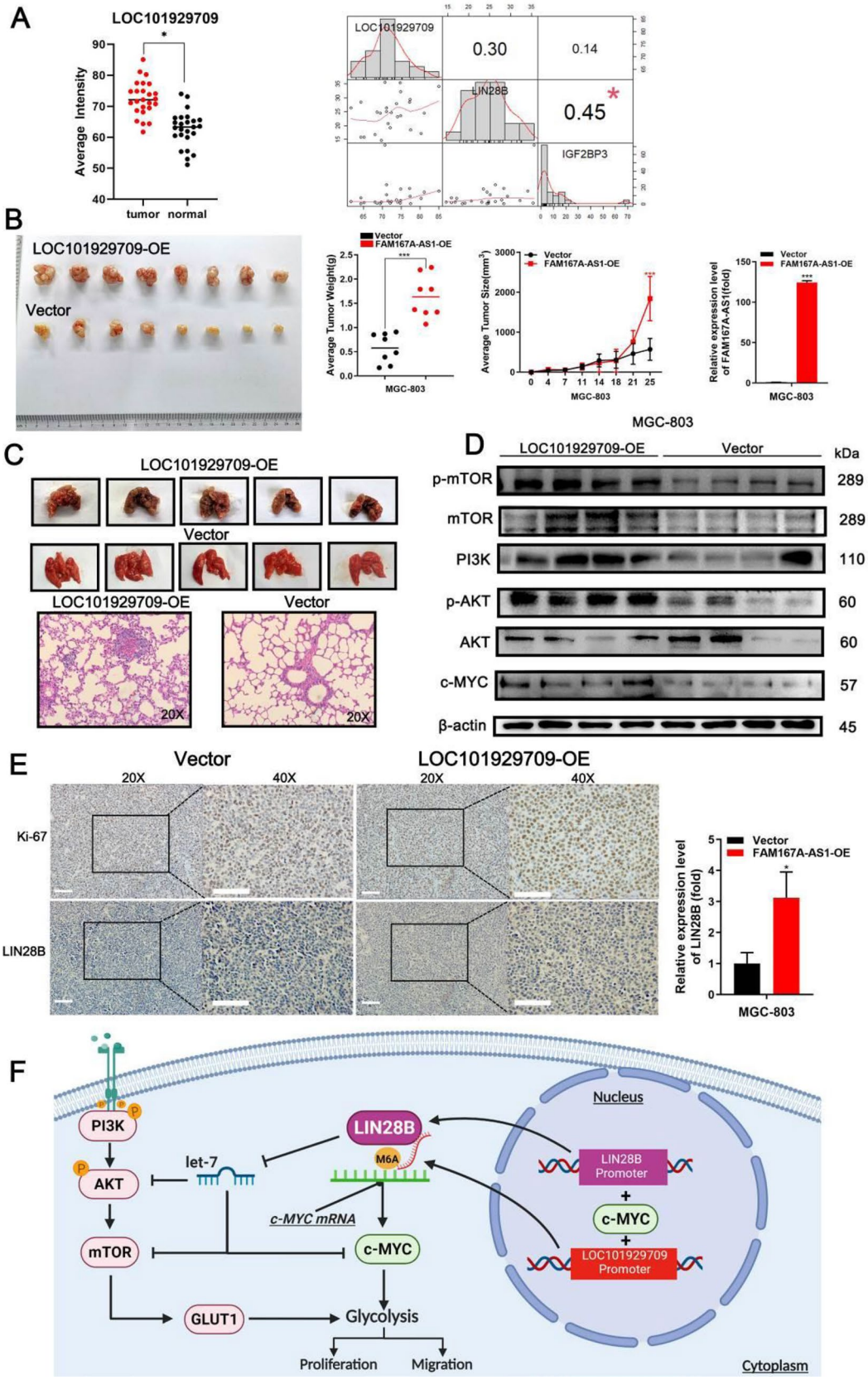
A
LOC101929709
Average Intensity
tumor
normal
LOC101929709
LIN28B
IGF2BP3
0.30
0.14
0.45
B
LOC101929709-OE
Vector
Vector
FAM167A-AS1-OE
Average Tumor Weight(g)
Average Tumor Size(mm3)
Relative expression level of FAM167A-AS1(fold)
MGC-803
C
LOC101929709-OE
Vector
20X
D
MGC-803
LOC101929709-OE
Vector
kDa
p-mTOR
mTOR
PI3K
p-AKT
AKT
c-MYC
β-actin
289
289
110
60
60
57
45
E
Vector
LOC101929709-OE
20X
40X
Ki-67
LIN28B
Relative expression level of LIN28B (fold)
F
PI3K
AKT
mTOR
let-7
LIN28B
M6A
c-MYC mRNA
c-MYC
GLUT1
Glycolysis
Proliferation
Migration
Nucleus
LIN28B Promoter
c-MYC
LOC101929709 Promoter
Cytoplasm

◂**Fig. 7** LOC101929709 promotes gastric cancer progression in vivo. **A** Expression of LOC101929709 in 25 pairs of gastric cancer tissues and matched adjacent normal tissues detected by FISH (left). Association of LOC101929709 and LIN28B and IGF2BP3 in 25 samples of gastric cancer. Correlation coefficient of LOC101929/LIN28B, LOC101929709/IGF2BP3, and LIN28B/IGF2BP3 is 0.30, 0.14, and 0.45, respectively. Corresponding p-values are 0.1519, 0.50, and 0.0242. **B** Representative images of subcutaneous tumours from mice injected with LOC101929709-OE cells (upper) or control cells (lower) on the left flank ($n=8$, each group). The mean weight of tumours is measured (left); tumour growth curves are drawn every 3 days until day 25 (middle); LOC101929709 expression in tumours is shown by qRT-PCR (right). **C** Representative images of lungs from LOC101929709-OE and control groups one month after tail vein injection ($n=5$, each group) (upper). Hematoxylin–eosin staining photos of different lungs (20× magnification) (lower). **D** Expression of proteins in primary tumours of LOC101929709-OE and control groups is shown by Western blot ($n=4$, each group). **E** Levels of c-MYC protein and Ki-67 index in LOC101929709-OE and NC groups are shown by IHC (20× and 40× magnification) (left); c-MYC mRNA in LOC101929709-OE and NC groups is shown by qRT-PCR (right). The data are presented as the mean of three independent experiments. Scale bars = 100 μm. $^{*}p<0.05$; $^{**}p<0.01$; $^{***}p<0.001$. Variables are presented as mean ± SD. **F** c-MYC binds to the promoters of both LIN28B and LOC101929709 to promote their transcription. LIN28B binds to c-MYC mRNA by recognizing m6A and maintaining its stability. Resultantly, LIN28B directly upregulates the expression of c-MYC to facilitate glycolysis. Moreover, LOC101929709 supports the binding between LIN28B and c-MYC mRNA. Additionally, LIN28B activates the PI3K/AKT pathway, which is important for glycolysis, by antagonizing let-7. Enhanced glycolysis is beneficial for the proliferation and migration of gastric cancer. Consequently, the c-MYC/LOC101929709/LIN28B axis induces the Warburg effect to accelerate tumour progression. Figure created using BioRender.com

translation [16, 39]. Furthermore, bioinformatics analysis and RIP-seq revealed that LIN28B binding sites partially overlapped with m6A modified regions, which is consistent with the fact that m6A plays a vital part in the binding between specific RBPs and their targets [23]. LIN28B has the potential to serve as an m6A reader as it binds to m6A modified RNA probes instead of unmethylated control. The specific structure of LIN28B that is mainly responsible for m6A recognition warrants further investigation.

Considering that LIN28B and IGF2BP3 can form an RNP complex, lncRNAs that are involved in the complex formation were screened for their potential to serve as a scaffold to enhance the binding between RBPs and mRNA [27, 40]. LOC101929709 was able to bind to both LIN28B and IGF2BP3 and its expression was positively associated with that of LIN28B in gastric cancer. LOC101929709 could bring LIN28B closer to c-MYC mRNA to inhibit c-MYC degradation. Consequently, the upregulation of c-MYC promoted the transcription of both LOC101929709 and LIN28B. By enhancing the function of LIN28B, LOC101929709 promoted multiple biological activities, including proliferation, migration and aerobic glycolysis. In principle, LOC101929709 functions as a scaffold for the interaction between c-MYC and LIN28B.

c-MYC and LIN28B collaborate to form a positive feedback loop [12]. The c-MYC/LIN28B axis can activate the PI3K/AKT pathway to promote tumour progression [10, 41]. Enlightened by this scenario, the c-MYC/LOC101929709/LIN28B axis was hypothesised: c-MYC transactivates LOC101929709 and LIN28B, which maintains the stability of c-MYC transcription. Furthermore, LOC101929709 guides LIN28B and c-MYC mRNA binding in the cytoplasm. Consequently, LIN28B activates the PI3K/AKT pathway. Thus, this circle facilitates the Warburg effect and promotes gastric cancer tumorigenesis (Fig. 7F).

The direct binding of LIN28B to c-MYC mRNA by recognising m6A modification provides a novel insight into the oncogenic role of LIN28B in gastric cancer. Therefore, repressing LOC101929709 could potentially block the c-MYC/LIN28B axis, inhibit the Warburg effect and suppress tumour progression. Thus, LOC101929709 serves as a potential new target for gastric cancer treatment.

Methods

Computational analysis

Target gene expression in tumour or normal tissues was obtained from The Cancer Genome Atlas (TCGA) and compared by UCSC Xena platform [42]. The RNA-seq data of GSE84437 and GSE62254 were downloaded from the Gene Expression Omnibus (GEO) database (https://www.ncbi.nlm.nih.gov/geo/). The link between TF and chromosome was predicted by JASPAR [43].

Cell culture

Gastric cancer cell lines (AGS, MKN1, SGC-7901, BGC-823, and MGC-803) and the gastric mucosal epithelial cell line GES-1 were purchased from China Center Type Culture Collection (CCTCC, Shanghai). AGS, BGC-823, and MGC-803 cell lines were cultured in DMEM. MKM1, SGC-7901 and GES-1 were cultured in RPMI 1640 (GIBCO, USA) medium supplemented with 10% fetal bovine serum (FBS), 100 U/ml penicillin and 100 mg/ml streptomycin (Invitrogen, USA) at 37 °C and 5% CO_2.

RNA extraction and quantitative real-time PCR (qRT-PCR) assay

Total RNAs were extracted by TRIZOL reagent (Invitrogen), or RNAeasy™ Plus Animal RNA Isolation Kit with Spin Column (Beyotime, China) following the instruction. For qRT-PCR, 1 μg of total RNA was reverse-transcribed by

the PrimeScriptP RT Reagent Kit (Takara, China). PCR was performed with SYBR Premix Ex Taq (Takara, China) in triplicate. The amplified transcript level of each specific gene was normalized to a constitutive expression gene β-actin. All primers (Supplementary Table S1) were provided by Geneseed Biotechnology Company (China) and Invitrogen.

RNA decay measurements

Cells transfected with different siRNAs were cultured in 6-well plates for 24 h (2×10^5/well). Transcription was inhibited by adding 2 μg/ml actinomycin D (MedChemExpress, USA). RNA was extracted every 20 min, until 1 h. RNAeasy™ Plus Animal RNA Isolation Kit was used to acquire RNA. Linear relationships were drawn by time as X-axis and amount of RNA as Y-axis.

Reagents

c-MYC inhibitors, 10,058-F4 and 10,074-G5 (Beyotime, China), were used at 15 μM for in vitro experiments. AKT inhibitors, AZD5363 and MK2206 (Beyotime, China), were used at 1 μM.

Plasmid construction and cell transfection

The full-length complementary DNAs (cDNAs) of human LOC101929709, c-MYC, LIN28B, and negative control (NC) were synthesized by Shanghai Genechem company using vector pcDNA3.1 (+). Plasmids were transfected into cells using the lipfectamine 3000 (Invitrogen) and siRNAs were transfected by Lipofectamine 2000 (Invitrogen) according to the manufacturer's instructions. All siRNA sequences are listed in Supplementary Table S1.

Lentivirus construction and cell infection

The control shRNA, LOC101929709 shRNA, LOC101929709 overexpression lentivirus were constructed by ShangHai GenePharma Company. Cells were infected with lentivirus for 3 days and treated with puromycin (1 μg/μl) for screening. When stable green fluorescence is observed by microscope, infected cell lines are constructed and confirmed by qRT-PCR or Western blot. We designed derivatives of MGC-803 and SGC-7901 with constitutive downregulation of LOC101929709 (LOC101929709-sh1/sh2) by lentivirus. LOC101929709-OE cell line was developed by LV5-LOC101929709.

Cell viability assays

Cells were seeded in 96-well plates (2×10^3/well) (5 holes/group). With the addition of 20 μl CCK-8 (Beyotime, China), light absorbance of the solution was measured at 450 nm. This examination was repeated every 24 h for 4 days. Cells for colony formation assay were seeded in 6-well plates at the density of 500 cells/well. After 14 days, cells were washed with PBS, fixed with 4% paraformaldehyde, stained with 0.1% crystal violet for 30 min and washed for twice. Colonies were photographed and counted under a light microscope. 5-Ethynyl-2′-deoxyuridine incorporation assays were conducted through the EdU assay kit (RiboBio, China) according to the manufacturer's instructions. Five fields of view were randomly selected for each sample at a 10× magnification. EdU-positive cells were stained with red dye, and the relative proliferation-positive ratios were calculated from the average cell count of the five visual fields at a 10× magnification.

Cell migration assays

For the wound healing assay, 4×10^5 cells were seeded in 6-well plates. After 24 h, a scratch was made by a 10 μl pipette tip. The bright-field images of the randomly selected views along the scraped lines were captured at 0, 12, and 24 h at a 10× magnification. Cells were incubated without FBS. The percent of the wounded area was calculated: (mean remained breadth/mean wounded breadth)×100(%). For the transwell assay, 5×10^4 cells were transferred to the upper chamber of an insert (8 μm pore size, Millipore). Medium with 10% FBS was added to the lower chamber. After 24 h, migrating cells were fixed by 95% ethanol, stained with 0.1% violet crystal for 15 min and photographed at a magnification of×10 under an inverted phase contrast microscope. The number was in five randomly selected microscopes.

Cell cycle assays

Flow cytometry was used to detected cell cycle distribution by FACS ARIA II SORP (BD Biosciences). Cells were harvested and stained by PI (Ebioscience, USA), and analyzed by fluorescence-activated cell sorting (FACS).

Protein extraction and Western blot

RIPA protein extraction reagent (Beyotime) supplemented with PMSF (Biosharp, China), was used to extract protein. The BCA protein assay kit (Beyotime) was used to determine the protein concentration. 15 μg of each kind of proteins was separated by 12% SDS-polyacrylamide gel electrophoresis (SDS-PAGE), transferred to 0.22 μm polyvinylidene fluoride membranes and incubated with nonfat dry milk, target or β-actin antibodies, and secondary antibodies in turn. Finally, results were detected by enhanced chemiluminescence (xinsaimei, China) reagent. Antibodies were purchased from manufacturers: Cell Signaling Technology (CST) (β-actin,

PI3K, p-AKT, AKT, p-mTOR, mTOR, LIN28B, IGF2BP3, and Flag) and Abcam (c-MYC).

Glucose uptake and lactate production assays

Cells were planted in culture media for 24 h, and then incubated with new media for an additional 24 h. Levels of intracellular glucose and lactate acid were assessed by the fluorescence-based glucose assay kit (NanJing JianCheng Bioengineering Institute, China) and lactic acid test kit (KeyGEN BioTECH, China) according to manufacturer's instructions. The sum of glucose uptake and lactate acid production was divided by cell number.

Seahorse extracellular flux assays

Extracellular acidification rate (ECAR) was measured in XF media under basal conditions and in response to glucose (10 mM), oligomycin (1 μM), and 2-DG (100 mM), using a Seahorse Biosciences Xfe 96 Flux Analyzer (North Billerica, MA). Oxygen consumption rate (OCR) was measured in response to oligo (1 μM), FCCP (3 μM) and antimycin (1 μM).

IF, FISH and subcellular fractionation

The IF assay was implemented by the Immunol Fluorescence Staining Kit following the directions (Beyotime, China). Simply, cells were fixed by 4% paraformaldehyde for 10 min and then permeabilized for 5 min by 0.5% Triton X-100. After washing by PBS, cells were blocked for 1 h and incubated with antibodies overnight and with fluorescent secondary antibodies for 2 h in the dark. DAPI was used for nuclear staining. Fixed cells were treated with Fluorescent In Situ Hybridization Kit (FISH) and probes (RiboBio) to show locations of RNA according to the manufacturer's instructions. Pictures were taken by the confocal laser scanning microscope at a 40× magnification. Separation of nuclear and cytosolic fractions was performed via the PARIS Kit (Life Technologies, USA) according to the manufacturer's instructions.

Co-immunoprecipitation assays

Protein extracts were incubated overnight with antibodies (LIN28B, #4196; IGF2BP3, #57,145) and Protein A/G PLUS-Agarose (Santa Curz, USA). Agarose was washed by lysis buffer and blended with SDS-PAGE buffer. Results of Co-immunoprecipitation (Co-IP) were detected by Western blot.

Chromatin immunoprecipitation assays

Chromatin immunoprecipitation (ChIP) experiments were performed using the EZ Magna ChIP Kit (Millipore, USA) according to the manufacturer's instructions. The anti-c-MYC antibody was purchased from Abcam (ab32072) and anti-H3K4ME2 antibody was obtained from CST (#9725). Primers of promoters are displayed in Supplementary Table S1.

RNA immunoprecipitation

RNA immunoprecipitation (RIP) experiments were performed by the EZ Magna RIP RNA-binding Protein Immunoprecipitation Kit (Millipore) with extracts of MGC-803. The anti-LIN28B, anti-IGF2BP3, anti-c-MYC, and anti-Flag antibodies were purchased from CST (#4196, #57,145, #18,583, # 14,793, 1:100). We detected co-precipitated RNAs by agarose gel electrophoresis and qRT-PCR. Total RNA and rabbit IgG controls were simultaneously assayed.

RIP-seq

RIP-seq was performed according to the classical instrument [44]. The procedure of RIP was mentioned above. QUBIT RNA HS assay kit (Invitrogen) was used to detect the concentration of LIN28B (3 ng/μl, 20 μl) and IGF2BP3 (7.5 ng/μl, 20 μl) samples. Agilent 2200 system with HS RNA Reagent (Invitrogen) was used for RNA quality control. Purified RIP RNAs were reverse transcribed into cDNA sequencing library using VAHTS Stranded mRNA-seq Library Prep kit Illumina (Vazyme, China). Libraries were sequenced via Nova platform (Illumina) with PE150 model (double-ended 150 bp sequencing). RIP-seq and subsequent bioinformatics Gene Ontology (GO) and Kyoto Encyclopedia of Genes and Genomes (KEGG) analysis were performed by RiboBio. Details of LIN28B/IGF2BP3 binding peaks, and KEGG/GO analysis are presented in Supplementary Table S2. Motif analysis of binding peaks was performed by MEME-ChIP [45].

RNA pull-down

We designed plasmids expressing LOC101929709 and synthesized the PCR primers of positive/negative-sense strand to obtain corresponding DNA templates by PCR amplification. Biotin-labeled LOC101929709 were in vitro transcribed with the Biotin RNA Labeling Mix and T7 RNA polymerase using a RNAmax-T7 biotin-labeled transcription Kit (RiboBio). The Pierce magnetic RNA–Protein Pull-down Kit (Thermo Fisher, USA) was used for extracting RNA/protein complexes. Biotin-labeled RNA was co-incubated with cell lysates on the shaker overnight and then incubated

with the mixed RNA–protein binding reaction solution for 1 h. RNA/protein complexes was eluted by buffer at 50 °C for 40 min. The proteins bound with LOC101929709 were detected by Western blot.

Luciferase reporter assay

Plasmids expressing firefly luciferase and customized promoters were constructed by Shanghai Genechem company using the vector GV208. Regions of mRNA were inserted into the 3'UTR of RLUC element on psiCHECK2 vectors. After transfection, cells were collected by Dual-Luciferase reporter assay kit (Promega, USA). Luciferase activity was measured using a BD Monolight 3010 luminometer (BD Biosciences). Results were normalized by dividing the Firefly luciferase (FLUC) activity to the corresponding Renilla luciferase (RLUC) activity. All sequences of designed promoters were listed in Supplementary Materials.

In vivo tumour growth assays

Four-week-old female athymic BALB/c nude mice were fed in the animal center of Nanjing Medical University. The cell mass (5×10^6) was dissolved in 200 µl PBS and subcutaneously injected into the left side of each mouse. Every 3 days, we calculated tumour volumes by measuring the longitudinal diameter and latitudinal diameter. Lung burden was detected one month after the tail vein injection with tumour cell suspension (1×10^6 cells/100 µl). The protocol was approved by the Committee on the Ethics of Animal Experiments of the Nanjing Medical University.

Immunohistochemical staining

The immunohistochemical (IHC) analysis was used to examine the expression of Ki67 and LIN28B by special antibodies (Ki67, servicebio, GB13030-2; LIN28B, CST, #4196). The dilution of primary antibodies was 1:100. Slides were examined independently by ImageJ. 35 gastric cancer tissues specimens and their adjacent normal tissues were used to make tissue microarray (TMA). TMAs were stained with anti-LIN28B antibody (Proteintech, China, #16,178–1-AP) or anti-IGF2BP3 antibody (Litho, China, #LTO4730), incubated with corresponding secondary antibodies. Furthermore, fluorescent probes targeting LOC101929709 were designed. The expression of LOC101929709 in TMA was also identified by FISH in 25 pairs of tissues.

Statistics

All the experiments in vitro were carried out in triplicate and repeated three times. Statistics significance in cell proliferation, migration and invasion assays was determined by a paired Student's t test, χ^2 test, Wilcoxon test, or One-way analysis of variance (ANOVA), as appropriate. The statistics analyses were calculated by the SPSS 17.0 statistical software package. Correlation analyses were performed using R software (version 4.1.1, www.r-project.org). p-value of no more than 0.05 was considered statistically significant. Results are from 1 representative experiment of 3 independent trials. Data are presented as means ± SD (SD). $*p<0.05$, $**p<0.01$, $***p<0.001$.

Supplementary Information The online version contains supplementary material available at https://doi.org/10.1007/s10120-022-01348-z.

Authors' contributions TY: investigation, writing—original draft. MX: visualization, formal analysis. YF: investigation, validation. TX: visualization. YP: supervision. PM: resources. YS: conceptualization, methodology. TX: Conceptualization, writing—review & editing.

Funding This study was supported by Jiangsu province 333 high level Talents Project (TP Xu), the Natural Science Foundation of Jiangsu Province (BK20211381 to TP Xu), the National Natural Science Foundation of China (82172889 to YQ Shu), Social development-key program-clinical frontier technology of Jiangsu Province (BE2020783 to YQ Shu).

Declarations

Conflict of interest The authors declare no potential conflicts of interest.

Availability of data and materials The datasets used and/or analyzed during the current study are available from the corresponding author on reasonable request.

Human and animal rights Animal experiments involved in this study were approved by the Committee on the Ethics of Animal Experiments of the Nanjing Medical University.

Consent for publication Not applicable.

References

1. Bray F, Ferlay J, Soerjomataram I, Siegel RL, Torre LA, Jemal A. Global cancer statistics 2018: GLOBOCAN estimates of incidence and mortality worldwide for 36 cancers in 185 countries. CA Cancer J Clin. 2018;68(6):394–424. https://doi.org/10.3322/caac.21492 (**PubMed PMID: 30207593**).
2. Yuan LW, Yamashita H, Seto Y. Glucose metabolism in gastric cancer: The cutting-edge. World J Gastroenterol. 2016;22(6):2046–59. https://doi.org/10.3748/wjg.v22.i6.2046 (**PubMed PMID: 26877609; PubMed Central PMCID: PMCPMC4726677**).
3. Sukumar M, Roychoudhuri R, Restifo NP. Nutrient competition: a new axis of tumour immunosuppression. Cell. 2015;162(6):1206–8. https://doi.org/10.1016/j.cell.2015.08.064 (**PubMed PMID: 26359979; PubMed Central PMCID: PMCPMC6327313**).
4. Yin C, Qie S, Sang N. Carbon source metabolism and its regulation in cancer cells. Crit Rev Eukaryot Gene Expr. 2012;22(1):17–35. https://doi.org/10.1615/critreveukargeneexpr.v22.i1.20 (**PubMed PMID: 22339657; PubMed Central PMCID: PMCPMC4505802**).

5. Ngo H, Tortorella SM, Ververis K, Karagiannis TC. The Warburg effect: molecular aspects and therapeutic possibilities. Mol Biol Rep. 2015;42(4):825–34. https://doi.org/10.1007/s11033-014-3764-7 (**PubMed PMID: 25253100**).
6. Chen C, Bai L, Cao F, Wang S, He H, Song M, et al. Targeting LIN28B reprograms tumour glucose metabolism and acidic microenvironment to suppress cancer stemness and metastasis. Oncogene. 2019;38(23):4527–39. https://doi.org/10.1038/s41388-019-0735-4 (**PubMed PMID: 30742065**).
7. Guo Y, Chen Y, Ito H, Watanabe A, Ge X, Kodama T, et al. Identification and characterization of lin-28 homolog B (LIN28B) in human hepatocellular carcinoma. Gene. 2006;384:51–61. https://doi.org/10.1016/j.gene.2006.07.011 (**PubMed PMID: 16971064**).
8. Hu Q, Peng J, Liu W, He X, Cui L, Chen X, et al. Lin28B is a novel prognostic marker in gastric adenocarcinoma. Int J Clin Exp Pathol. 2014;7(8):5083–9 (**PubMed PMID: 25197381; PubMed Central PMCID: PMCPMC4152071**).
9. Zhang X, Liang W, Liu J, Zang X, Gu J, Pan L, et al. Long non-coding RNA UFC1 promotes gastric cancer progression by regulating miR-498/Lin28b. J Exp Clin Cancer Res. 2018;37(1):134. https://doi.org/10.1186/s13046-018-0803-6 (**PubMed PMID: 29970131; PubMed Central PMCID: PMCPMC6029056**).
10. Wang T, Wang G, Hao D, Liu X, Wang D, Ning N, et al. Aberrant regulation of the LIN28A/LIN28B and let-7 loop in human malignant tumours and its effects on the hallmarks of cancer. Mol Cancer. 2015;14:125. https://doi.org/10.1186/s12943-015-0402-5 (**PubMed PMID: 26123544; PubMed Central PMCID: PMCPMC4512107**).
11. Boyerinas B, Park SM, Hau A, Murmann AE, Peter ME. The role of let-7 in cell differentiation and cancer. Endocr Relat Cancer. 2010;17(1):F19-36. https://doi.org/10.1677/ERC-09-0184 (**PubMed PMID: 19779035**).
12. Wu G, Huang P, Ju X, Li Z, Wang Y. Lin28B over-expression mediates the repression of let-7 by hepatitis B virus X protein in hepatoma cells. Int J Clin Exp Med. 2015;8(9):15108–16 (**PubMed PMID: 26628994; PubMed Central PMCID: PMCPMC4658883**).
13. Dang CV. MYC, metabolism, cell growth, and tumourigenesis. Cold Spring Harb Perspect Med. 2013. https://doi.org/10.1101/cshperspect.a014217 (**PubMed PMID: 23906881; PubMed Central PMCID: PMCPMC3721271**).
14. Chang TC, Zeitels LR, Hwang HW, Chivukula RR, Wentzel EA, Dews M, et al. Lin-28B transactivation is necessary for Myc-mediated let-7 repression and proliferation. Proc Natl Acad Sci U S A. 2009;106(9):3384–9. https://doi.org/10.1073/pnas.0808300106 (**PubMed PMID: 19211792; PubMed Central PMCID: PMCPMC2651245**).
15. Wang S, Chim B, Su Y, Khil P, Wong M, Wang X, et al. Enhancement of LIN28B-induced hematopoietic reprogramming by IGF2BP3. Genes Dev. 2019;33(15–16):1048–68. https://doi.org/10.1101/gad.325100.119 (**PubMed PMID: 31221665; PubMed Central PMCID: PMCPMC6672051**).
16. Huang H, Weng H, Sun W, Qin X, Shi H, Wu H, et al. Recognition of RNA N(6)-methyladenosine by IGF2BP proteins enhances mRNA stability and translation. Nat Cell Biol. 2018;20(3):285–95. https://doi.org/10.1038/s41556-018-0045-z (**PubMed PMID: 29476152; PubMed Central PMCID: PMCPMC5826585**).
17. Dykes IM, Emanueli C. Transcriptional and post-transcriptional gene regulation by long non-coding RNA. Genom Proteom Bioinform. 2017;15(3):177–86. https://doi.org/10.1016/j.gpb.2016.12.005 (**PubMed PMID: 28529100; PubMed Central PMCID: PMCPMC5487525**).
18. Geisler S, Coller J. RNA in unexpected places: long non-coding RNA functions in diverse cellular contexts. Nat Rev Mol Cell Biol. 2013;14(11):699–712. https://doi.org/10.1038/nrm3679 (**PubMed PMID: 24105322; PubMed Central PMCID: PMCPMC4852478**).
19. Huang J, Zhang A, Ho TT, Zhang Z, Zhou N, Ding X, et al. LincRoR promotes c-Myc expression through hnRNP I and AUF1. Nucleic Acids Res. 2016;44(7):3059–69. https://doi.org/10.1093/nar/gkv1353 (**PubMed PMID: 26656491; PubMed Central PMCID: PMCPMC4838338**).
20. Xu TP, Liu XX, Xia R, Yin L, Kong R, Chen WM, et al. SP1-induced upregulation of the long noncoding RNA TINCR regulates cell proliferation and apoptosis by affecting KLF2 mRNA stability in gastric cancer. Oncogene. 2015;34(45):5648–61. https://doi.org/10.1038/onc.2015.18 (**PubMed PMID: 25728677**).
21. Hafner M, Max KE, Bandaru P, Morozov P, Gerstberger S, Brown M, et al. Identification of mRNAs bound and regulated by human LIN28 proteins and molecular requirements for RNA recognition. RNA. 2013;19(5):613–26. https://doi.org/10.1261/rna.036491.112 (**PubMed PMID: 23481595; PubMed Central PMCID: PMCPMC3677277**).
22. Graf R, Munschauer M, Mastrobuoni G, Mayr F, Heinemann U, Kempa S, et al. Identification of LIN28B-bound mRNAs reveals features of target recognition and regulation. RNA Biol. 2013;10(7):1146–59. https://doi.org/10.4161/rna.25194 (**PubMed PMID: 23770886; PubMed Central PMCID: PMCPMC3849162**).
23. Meyer KD, Saletore Y, Zumbo P, Elemento O, Mason CE, Jaffrey SR. Comprehensive analysis of mRNA methylation reveals enrichment in 3' UTRs and near stop codons. Cell. 2012;149(7):1635–46. https://doi.org/10.1016/j.cell.2012.05.003 (**PubMed PMID: 22608085; PubMed Central PMCID: PMCPMC3383396**).
24. Dominissini D, Moshitch-Moshkovitz S, Schwartz S, Salmon-Divon M, Ungar L, Osenberg S, et al. Topology of the human and mouse m6A RNA methylomes revealed by m6A-seq. Nature. 2012;485(7397):201–6. https://doi.org/10.1038/nature11112 (**PubMed PMID: 22575960**).
25. Wang X, Sun L, Wang X, Kang H, Ma X, Wang M, et al. Acidified bile acids enhance tumour progression and telomerase activity of gastric cancer in mice dependent on c-Myc expression. Cancer Med. 2017;6(4):788–97. https://doi.org/10.1002/cam4.999 (**PubMed PMID: 28247570; PubMed Central PMCID: PMC5387128**).
26. Aksoz M, Albayrak E, Aslan GS, Turan RD, Alyazici LY, Siyah P, et al. c-Myc inhibitor 10074–G5 induces murine and human hematopoietic stem and progenitor cell expansion and HDR modulator Rad51 expression. Curr Cancer Drug Targets. 2019;19(6):479–94. https://doi.org/10.2174/1568009618666180905100608 (**PubMed PMID: 30182856**).
27. Zhang S, Zhao BS, Zhou A, Lin K, Zheng S, Lu Z, et al. m(6)A demethylase ALKBH5 maintains tumourigenicity of glioblastoma stem-like cells by sustaining FOXM1 expression and cell proliferation program. Cancer Cell. 2017;31(4):591-606e6. https://doi.org/10.1016/j.ccell.2017.02.013 (**PubMed PMID: 28344040; PubMed Central PMCID: PMC5427719**).
28. Nukina K, Hayashi A, Shiomi Y, Sugasawa K, Ohtsubo M, Nishitani H. Mutations at multiple CDK phosphorylation consensus sites on Cdt2 increase the affinity of CRL4(Cdt2) for PCNA and its ubiquitination activity in S phase. Genes Cells. 2018;23(3):200–13. https://doi.org/10.1111/gtc.12563 (**PubMed PMID: 29424068**).
29. Zhu H, Shyh-Chang N, Segre AV, Shinoda G, Shah SP, Einhorn WS, et al. The Lin28/let-7 axis regulates glucose metabolism. Cell. 2011;147(1):81–94. https://doi.org/10.1016/j.cell.2011.08.033 (**PubMed PMID: 21962509; PubMed Central PMCID: PMCPMC3353524**).
30. Liu J, Feng W, Liu M, Rao H, Li X, Teng Y, et al. Stomach-specific c-Myc overexpression drives gastric adenoma in mice

through AKT/mammalian target of rapamycin signaling. Bosn J Basic Med Sci. 2021;21(4):434–46. https://doi.org/10.17305/bjbms.2020.4978 (**PubMed PMID: 33259779; PubMed Central PMCID: PMC8292868**).
31. Schaub FX, Dhankani V, Berger AC, Trivedi M, Richardson AB, Shaw R, et al. Pan-cancer alterations of the MYC oncogene and its proximal network across the cancer genome atlas. Cell Syst. 2018;6(3):282-300e2. https://doi.org/10.1016/j.cels.2018.03.003.
32. Lee BK, Bhinge AA, Battenhouse A, McDaniell RM, Liu Z, Song L, et al. Cell-type specific and combinatorial usage of diverse transcription factors revealed by genome-wide binding studies in multiple human cells. Genome Res. 2012;22(1):9–24. https://doi.org/10.1101/gr.127597.111 (**PubMed PMID: 22090374; PubMed Central PMCID: PMC3246210**).
33. Hanahan D, Weinberg RA. Hallmarks of cancer: the next generation. Cell. 2011;144(5):646–74. https://doi.org/10.1016/j.cell.2011.02.013 (**PubMed PMID: 21376230**).
34. Yang L, Zhang W, Wang Y, Zou T, Zhang B, Xu Y, et al. Hypoxia-induced miR-214 expression promotes tumour cell proliferation and migration by enhancing the Warburg effect in gastric carcinoma cells. Cancer Lett. 2018;414:44–56. https://doi.org/10.1016/j.canlet.2017.11.007 (**PubMed PMID: 29129783**).
35. Yu T, Wang Y, Fan Y, Fang N, Wang T, Xu T, et al. CircRNAs in cancer metabolism: a review. J Hematol Oncol. 2019;12(1):90. https://doi.org/10.1186/s13045-019-0776-8 (**PubMed PMID: 31484561; PubMed Central PMCID: PMCPMC6727394**).
36. Benhamou D, Labi V, Novak R, Dai I, Shafir-Alon S, Weiss A, et al. A c-Myc/miR17-92/Pten axis controls PI3K-mediated positive and negative selection in B cell development and reconstitutes CD19 deficiency. Cell Rep. 2016;16(2):419–31. https://doi.org/10.1016/j.celrep.2016.05.084 (**PubMed PMID: 27346348**).
37. Wilbert ML, Huelga SC, Kapeli K, Stark TJ, Liang TY, Chen SX, et al. LIN28 binds messenger RNAs at GGAGA motifs and regulates splicing factor abundance. Mol Cell. 2012;48(2):195–206. https://doi.org/10.1016/j.molcel.2012.08.004 (**PubMed PMID: 22959275; PubMed Central PMCID: PMCPMC3483422**).
38. Vanhee S, Akerstrand H, Kristiansen TA, Datta S, Montano G, Vergani S, et al. Lin28b controls a neonatal to adult switch in B cell positive selection. Sci Immunol. 2019. https://doi.org/10.1126/sciimmunol.aax4453 (**PubMed PMID: 31562190**).
39. Weidensdorfer D, Stohr N, Baude A, Lederer M, Kohn M, Schierhorn A, et al. Control of c-myc mRNA stability by IGF2BP1-associated cytoplasmic RNPs. RNA. 2009;15(1):104–15. https://doi.org/10.1261/rna.1175909 (**PubMed PMID: 19029303; PubMed Central PMCID: PMCPMC2612774**).
40. Yang JH, Chang MW, Pandey PR, Tsitsipatis D, Yang X, Martindale JL, et al. Interaction of OIP5-AS1 with MEF2C mRNA promotes myogenic gene expression. Nucleic Acids Res. 2020;48(22):12943–56. https://doi.org/10.1093/nar/gkaa1151 (**PubMed PMID: 33270893; PubMed Central PMCID: PMC7736780**).
41. Chen Q, Shen H, Zhu X, Liu Y, Yang H, Chen H, et al. A nuclear lncRNA Linc00839 as a Myc target to promote breast cancer chemoresistance via PI3K/AKT signaling pathway. Cancer Sci. 2020;111(9):3279–91. https://doi.org/10.1111/cas.14555 (**PubMed PMID: 32619088; PubMed Central PMCID: PMC7469761**).
42. Goldman MJ, Craft B, Hastie M, Repecka K, McDade F, Kamath A, et al. Visualizing and interpreting cancer genomics data via the Xena platform. Nat Biotechnol. 2020;38(6):675–8. https://doi.org/10.1038/s41587-020-0546-8 (**PubMed PMID: 32444850; PubMed Central PMCID: PMC7386072**).
43. Fornes O, Castro-Mondragon JA, Khan A, van der Lee R, Zhang X, Richmond PA, et al. JASPAR 2020: update of the open-access database of transcription factor binding profiles. Nucleic Acids Res. 2020;48(D1):D87–92. https://doi.org/10.1093/nar/gkz1001 (**PubMed PMID: 31701148; PubMed Central PMCID: PMCPMC7145627**).
44. Ye M, Xie L, Zhang J, Liu B, Liu X, He J, et al. Determination of long non-coding RNAs associated with EZH2 in neuroblastoma by RIP-seq, RNA-seq and ChIP-seq. Oncol Lett. 2020;20(4):1. https://doi.org/10.3892/ol.2020.11862 (**PubMed PMID: 32774475; PubMed Central PMCID: PMC7405546**).
45. Machanick P, Bailey TL. MEME-ChIP: motif analysis of large DNA datasets. Bioinformatics. 2011;27(12):1696–7. https://doi.org/10.1093/bioinformatics/btr189 (**PubMed PMID: 21486936; PubMed Central PMCID: PMC3106185**).